www.nature.com/cr
www.cell-research.com

Cell Research

ARTICLE

An NF90/NF110-mediated feedback amplification loop regulates dicer expression and controls ovarian carcinoma progression

Jérôme Barbier[1], Xin Chen[1,2], Gabriel Sanchez[1], Muyan Cai[2], Marion Helsmoortel[1], Takuma Higuchi[3], Pierre Giraud[1], Xavier Contreras[1], Gangjun Yuan[2], Zihao Feng[4], Rima Nait-Saidi[1], Olivier Deas[5], Lisa Bluy[1], Jean-Gabriel Judde[5], Sylvie Rouquier[1], William Ritchie[6], Shuji Sakamoto[3], Dan Xie[2] and Rosemary Kiernan[1]

Reduced expression of DICER, a key enzyme in the miRNA pathway, is frequently associated with aggressive, invasive disease, and poor survival in various malignancies. Regulation of DICER expression is, however, poorly understood. Here, we show that NF90/NF110 facilitates DICER expression by controlling the processing of a miRNA, miR-3173, which is embedded in DICER pre-mRNA. As miR-3173 in turn targets NF90, a feedback amplification loop controlling DICER expression is established. In a nude mouse model, NF90 overexpression reduced proliferation of ovarian cancer cells and significantly reduced tumor size and metastasis, whereas overexpression of miR-3173 dramatically increased metastasis in an NF90- and DICER-dependent manner. Clinically, low NF90 expression and high miR-3173-3p expression were found to be independent prognostic markers of poor survival in a cohort of ovarian carcinoma patients. These findings suggest that, by facilitating DICER expression, NF90 can act as a suppressor of ovarian carcinoma.

Cell Research (2018) 28:556–571; https://doi.org/10.1038/s41422-018-0016-8

INTRODUCTION

Ovarian cancer has the highest prevalence among gynecological cancers worldwide with >200,000 newly diagnosed cases and 150,000 reported deaths per year.[1,2] Although current therapies are highly effective in the treatment of early-stage cancer,[3] they are much less efficient in the treatment of advanced disease. Indeed, only about 30% of ovarian cancer patients with advanced-stage disease survive >5 years after initial diagnosis.[4] A compounding factor in the high mortality rate is that ovarian cancer spreads by direct invasion to adjacent organs or by transport throughout the peritoneal cavity.[5] Despite a good response to platinum and taxane post-operative therapies, most advanced-stage patients eventually die of disease recurrence.[3,4] Thus, the lack of an early screening strategy[6] and the frequency of tumor relapse[7] contribute to the high mortality rate in ovarian cancer patients. A better understanding of the mechanisms involved in ovarian cancer progression and invasion are required in order to develop targeted treatment strategies.

RNA interference (RNAi) is a highly conserved mechanism that modulates gene expression by posttranscriptional gene silencing in the cytoplasm. In the canonical pathway, the consecutive actions of two RNase III enzymes: DROSHA and DICER generate microRNAs (miRNAs), an abundant class of noncoding RNAs approximately 22 nucleotides (nt) in length. DROSHA, together with its cofactor DiGeorge syndrome critical region 8 (DGCR8), forms a complex known as Microprocessor[8–10] that cleaves primary miRNAs (pri-miRNAs) to release short hairpin precursors (pre-miRNAs).[11] Following export to the cytoplasm, pre-miRNAs are subsequently processed by DICER to yield mature miRNA duplexes.[12–15] Mature miRNAs are loaded onto the Argonaute-containing, RNA-induced silencing complex (RISC) to target complementary mRNA for degradation or inhibition of translation.[16] MiRNAs are predicted to regulate the expression of >60% of mammalian genes,[16] and consequently, to play fundamental roles in most biological processes, as well as in multiple diseases including cancer.[17]

Early clinical findings demonstrated that miRNA levels are frequently reduced in tumors.[18] In accordance with these observations, several members of the miRNA pathway, including DICER and XPO5, have been identified as haploinsufficient tumor suppressors in mice.[18–23] Using model systems in vitro, down-regulation of DICER has been shown to stimulate metastasis.[21,23] In patients, low levels of DICER in breast, ovarian, and other cancers are associated with aggressive invasive disease, distant recurrence, and poor survival.[24–27]

[1]Institut de Génétique Humaine, CNRS, University of Montpellier, Gene Regulation Laboratory, 141 rue de la cardonille, Montpellier, France; [2]State Key Laboratory of Oncology in South China, Collaborative Innovation Center for Cancer Medicine, Sun Yat-sen University Cancer Center, Guangzhou 510060, China; [3]Laboratory of Molecular Biology, Science Research Center, Kochi Medical School, Kochi University, Kochi 783-8505, Japan; [4]The First Affiliated Hospital, Sun Yat-sen University, Guangzhou 510060, China; [5]XenTech SAS, 4 rue Pierre Fontaine, Evry 91000, France and [6]Institut de Génétique Humaine, CNRS, University of Montpellier, Machine Learning and Gene Regulation Laboratory, 141 rue de la cardonille, Montpellier 34396, France
Correspondence: Dan Xie (xiedan@sysucc.org.cn) or Rosemary Kiernan (Rosemary.Kiernan@igh.cnrs.fr)
These authors contributed equally: Jérôme Barbier, Xin Chen and Gabriel Sanchez.

Received: 21 September 2017 Revised: 26 January 2018 Accepted: 28 January 2018
Published online: 21 March 2018

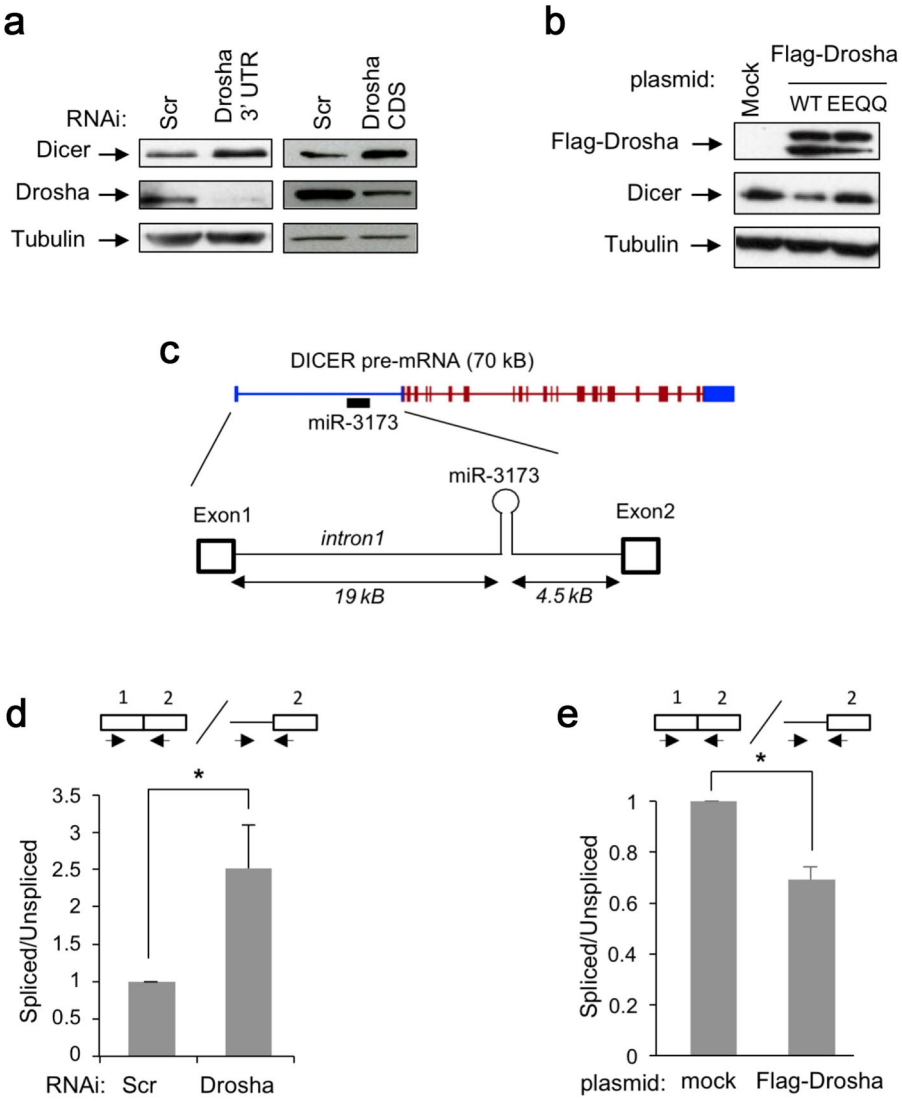

Fig. 1 Microprocessor modulates the splicing efficiency and expression level of DICER. **a** RNAi against DROSHA increases the expression level of DICER. Extracts of 293T cells transfected with DROSHA-specific or a non-targeting control siRNA were analyzed by immunoblot using the antibodies indicated. **b** 293T cells transfected with a plasmid expressing wild-type or catalytic mutant (EEQQ) Flag-DROSHA were analyzed by immunoblot using the antibodies indicated. **c** Schematic representing DICER pre-mRNA showing the location of miR-3173 within the first intron. Blue lines represent the UTRs, red lines represent the CDS. Exons are shown as boxes, introns as horizontal lines. **d** Extracts of control or DROSHA knock-down 293T cells were analyzed by RT-qPCR using PCR primers specifically amplifying spliced or unspliced transcripts. The splicing efficiency was calculated by the ratio of spliced to unspliced transcripts. Values obtained for the control sample (siScr) were attributed a value of 1. Data represent mean ± SEM obtained from three independent experiments (*$P < 0.05$, independent Student's *t*-test). **e** Analysis of splicing efficiency calculated as in **d** was performed using extracts of control cells or cells overexpressing Flag-DROSHA. Data represent mean ± SEM obtained from three independent experiments (*$P < 0.05$, independent Student's *t*-test)

Surprisingly, relatively little is known about the mechanisms that regulate DICER expression. MITF, TAp63, Sox4, and cyclin D1 have been shown to modulate DICER transcription through binding to cognate sites in the DICER promoter.[23,28–30] Additionally, several miRNAs, including miR-103/107, miR-192, and members of the Let-7 family, are known to modulate DICER post-transcriptionally by binding to target sites in the 3′-UTR of DICER mRNA.[21,31,32] DICER expression is also suppressed epigenetically during hypoxia.[33]

The interleukin enhancer binding factor 3 gene produces a protein product NF90 and its isoforms, including the longer isoform, NF110. NF90 is a double-stranded RNA (dsRNA)-binding protein that complexes with other proteins, dsRNAs, small noncoding RNAs, and mRNAs to regulate gene expression and stabilize mRNAs and has been shown to have numerous functions in RNA biology and viral replication.[34] NF90, together with its partner NF45, has been shown to negatively affect the processing of a number of miRNAs through competition with Microprocessor for binding to the pri-miR.[35,36]

Here, we describe a novel regulation of DICER expression that is mediated by a feedback amplification loop and that significantly impacts on ovarian carcinoma progression. We show that DICER expression is controlled by NF90/NF110. DICER hosts a miRNA, miR-3173, within the first intron of DICER pre-mRNA, which acts as a control point for DICER expression. NF90/NF110 enhances splicing efficiency and expression of DICER and disfavors pri-miR-3173 processing. Our results indicate that a feedback amplification loop is established through the mature miR-3173-3p that in turn targets NF90 mRNA thereby diminishing the abundance of NF90, and consequently, DICER. In clinical samples, high levels of NF90

and DICER were correlated with better survival in ovarian carcinoma patients. In primary ovarian carcinoma cells, overexpression of NF90 led to an increase in the level of DICER expression and reduced cell proliferation. In a nude mouse model, NF90 overexpression significantly reduced tumor size and metastasis. In contrast, overexpression of miR-3173 dramatically increased metastasis in an NF90- and DICER-dependent manner. Analysis of a cohort of ovarian carcinoma patients showed that low expression of NF90 and high expression of miR-3173-3p are independent prognostic markers of poor survival of the disease. Together, these results open new avenues for potential therapeutic approaches in the treatment of ovarian carcinoma.

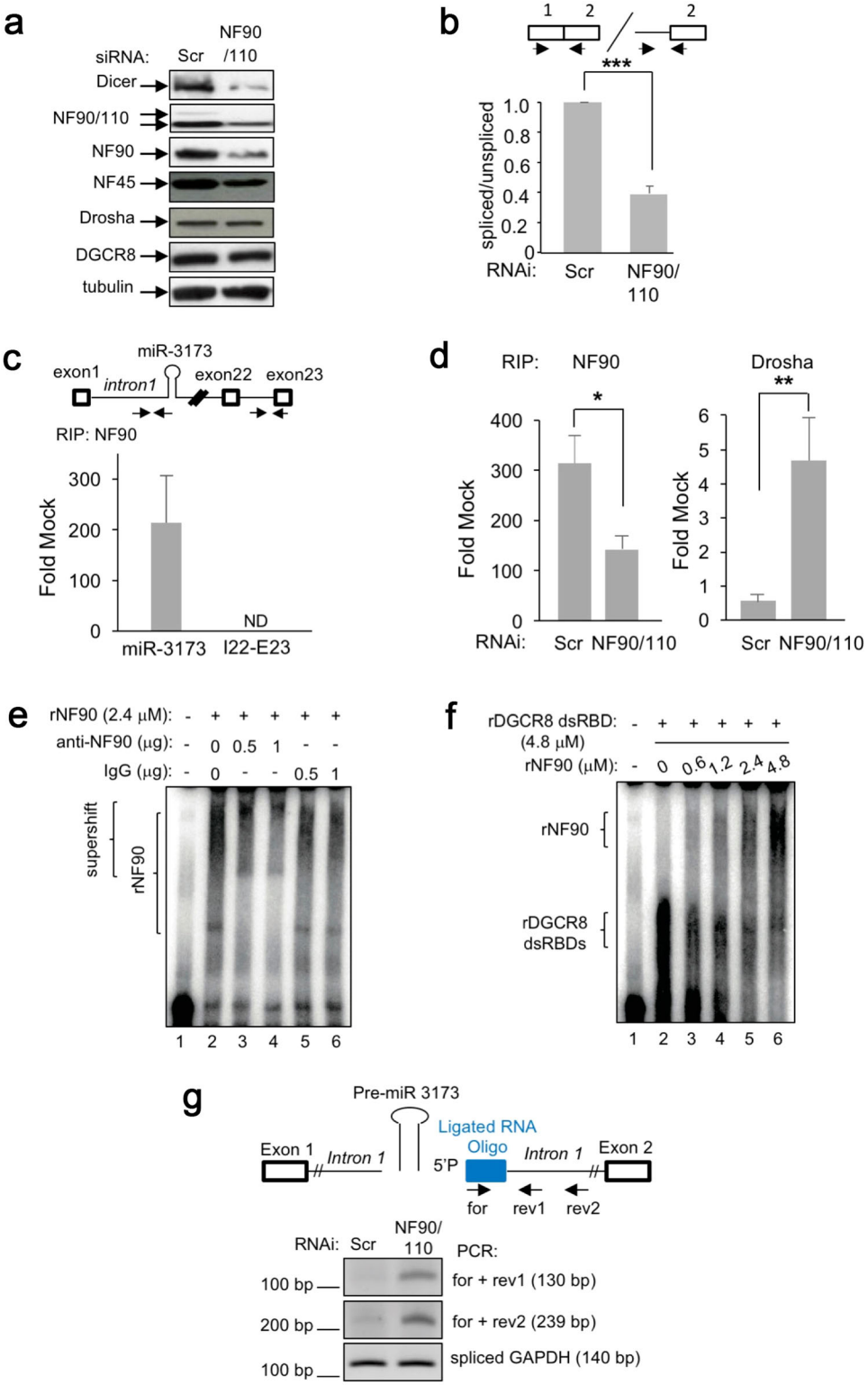

Fig. 2 NF90/NF110 affects DICER splicing efficiency and expression level by modulating recruitment of Microprocessor to pri-miR-3173. **a** RNAi against NF90/NF110 diminishes DICER expression level. Extracts of 293T cells transfected with control of NF90/110-specific siRNA were analyzed by immunoblot using the antibodies indicated. **b** Extracts of control or NF90/NF110 knock-down cells were analyzed by RT-qPCR using PCR primers amplifying spliced or unspliced transcripts. The splicing efficiency was calculated by the ratio of spliced to unspliced transcripts. Values obtained for the control sample (siScr) were attributed a value of 1. Data represent mean ± SEM obtained from three independent experiments (***$P < 0.001$, independent Student's *t*-test). **c** NF90 associates with the miR-3173 within DICER pre-mRNA. 293T cells were subjected to RIP using anti-NF90 or a control antibody. Immunoprecipitates were analyzed by RT-qPCR using the primers indicated on the schematic shown above the graph. Data represent fold increase over IgG control samples (mean ± SEM obtained from at least three independent experiments). ND indicates 'not detected'. **d** NF90/NF110 modulates association of DROSHA with the region proximal to miR-3173. 293T cells transfected with control or NF90/NF110-specific siRNA were analyzed by RIP using antibody to NF90, DROSHA or a control IgG as indicated. Immunoprecipitates were analyzed by RT-qPCR using primers to amplify the region proximal to miR-3173. Data represent fold increase over IgG control samples (mean ± SEM obtained from three independent experiments, **$P < 0.01$, *$P < 0.05$, independent Student's *t*-test). **e** RNA EMSA performed using recombinant NF90 (rNF90), alone or together with the antibodies indicated on the figure, was probed with radio-labelled pri-miR-3173. rNF90-pri-miR-3173 complexes and super-shifted complexes are indicated on the figure. **f** RNA EMSA performed using 4.8 μM recombinant DGCR8 dsRNA binding domain (amino acids 484–773), either alone or together with increasing amounts of rNF90 and probed with radio-labelled pri-miR-3173. **g** NF90/NF110 modulates cleavage of pre-Dicer mRNA at the region containing miR-3173. 293T cells transfected with control or NF90/NF110-specific siRNA were analyzed by modified 5′-RLM RACE. Forward (for) and reverse primers (rev1 and rev2) used, and the predicted sizes of the PCR products are indicated

RESULTS

Expression of DICER is regulated by Microprocessor through modulation of pre-mRNA splicing efficiency

We have previously shown that Microprocessor can regulate the expression of HIV and human genes through processing of stem loop structures embedded in the 5′-UTR of transcripts.[37] During this study, we observed that the expression of DICER was negatively affected by Microprocessor. Knock-down of DROSHA using two different DROSHA-specific small interfering RNAs (siRNAs) resulted in increased expression of DICER in two different human cell lines (Fig. 1a and Supplementary information, Figure S1A). Expression of DICER was also increased following loss of DROSHA's cofactor, DGCR8 (Supplementary information, Figure S1B). To determine whether the effect of Microprocessor required its catalytic activity, expression of DICER was analyzed in cells overexpressing either wild-type (WT) or a catalytically inactive mutant (E1045Q/E1222Q) of DROSHA.[10] Expression of DICER was diminished by WT, but not by mutant (EEQQ) DROSHA (Fig. 1b), indicating that the effect on DICER expression requires the catalytic activity of Microprocessor.

To determine whether the effect of Microprocessor on DICER was mediated through the canonical miRNA pathway, we analyzed the effect of knock-down of several key factors in the cytoplasmic RNAi pathway. Loss of AGO2, p54/Rck, XRN1, or LSM1 had no significant effect on DICER expression (Supplementary information, Figure S1C), suggesting that the effect of Microprocessor on DICER expression is not due to modulation of one or more miRNAs that target sites in the 3′-UTR of the Dicer mRNA.

To understand how Microprocessor modulates DICER expression, we checked whether DICER pre-mRNA may contain potential Microprocessor substrates whose cropping may have an impact upon DICER expression. Indeed, a miRNA, hsa-mir-3173, has been described in the first intron of DICER within the 5′-UTR (Fig. 1c). To investigate whether cropping of miR-3173 from the intron by Microprocessor may have an impact on splicing, we performed reverse transcription quantitative PCR assays to analyze the effect of Microprocessor on the splicing efficiency of DICER pre-mRNA. In the absence of DROSHA, the splicing efficiency of DICER pre-mRNA was enhanced by 2.5-fold as measured by the ratio of spliced/unspliced intermediates (Fig. 1d and Supplementary information, Figure S1D-E). In contrast, overexpression of Microprocessor diminished the splicing efficiency of DICER (Fig. 1e). This effect does not appear to be the result of a global effect of Microprocessor on splicing for three reasons. First, Microprocessor did not affect the splicing efficiency of Dicer pre-mRNA further downstream at exon 7 (data not shown). Second, the cropping of certain intron-embedded miRNAs has been shown to be compatible with splicing of the intron.[38,39] When splicing analysis of the previously identified host genes was performed using the same cell extracts used in Fig. 1d, similar results to these previous studies were obtained, which show that splicing of these miRNA-containing introns was not enhanced by loss of Drosha (Supplementary information, Figure S1F-G). Third, splicing of other genes that do not contain miRNAs, such as GAPDH, was not affected by loss of Microprocessor (Supplementary information, Figure S1H). Thus, Microprocessor diminishes pre-mRNA splicing efficiency of DICER and the effects observed on splicing are consistent with those observed on DICER protein expression.

NF90/NF110 regulates DICER expression by modulating recruitment of Microprocessor to DICER pre-mRNA

Microprocessor has been shown to associate with accessory complexes that can influence the processing of pri-miRs either positively or negatively.[9,35] NF90 is part of a dsRNA-binding protein complex that has been shown to reduce the processing efficiency of several miRNAs by Microprocessor.[34–36,40] We therefore analyzed the effect of NF90 on DICER expression. In contrast to that of DROSHA, knock-down of NF90 and the longer isoform, NF110 diminished the expression of DICER (Fig. 2a, Supplementary information, Figure S2A). Specific knock-down of the NF90 isoform also diminished expression of DICER (Supplementary information, Figure S2B). RNAi against the NF110 isoform alone was unsuccessful and so its effect on DICER expression cannot be determined. Loss of NF90/NF110 did not affect the expression of Microprocessor subunits DROSHA or DGCR8 but did induce destabilization of its partner NF45, as reported previously[41] (Fig. 2a). Our results therefore suggest that at least NF90 can affect DICER expression and a role for NF110 cannot be excluded.

Splicing analysis revealed that NF90/NF110 knock-down reduced the splicing efficiency of DICER by more than twofold (Fig. 2b and Supplementary information, Figure S2C) but did not affect the splicing of other introns hosting miRNAs (Supplementary information, Figure S2D). As NF90 has been shown to act as a transcription factor for interleukin 2,[41] we first excluded the possibility that loss of NF90/NF110 affected transcription of DICER, which could potentially induce splicing defects. Chromatin immunoprecipitation (ChIP) analysis of the promoter region of DICER showed that association of RNAPII was not affected by NF90/NF110 (Supplementary information, Figure S2E). NF90 has been shown to compete with Microprocessor and prevent processing of some pri-miRNAs.[35,36] We then wondered whether NF90/NF110 promotes splicing of DICER pre-mRNA by impeding the processing of pri-miR-3173 by Microprocessor, which could result in more efficient splicing of the intron in which pri-miR-3173 is localized. Thus, we first determined whether NF90 directly

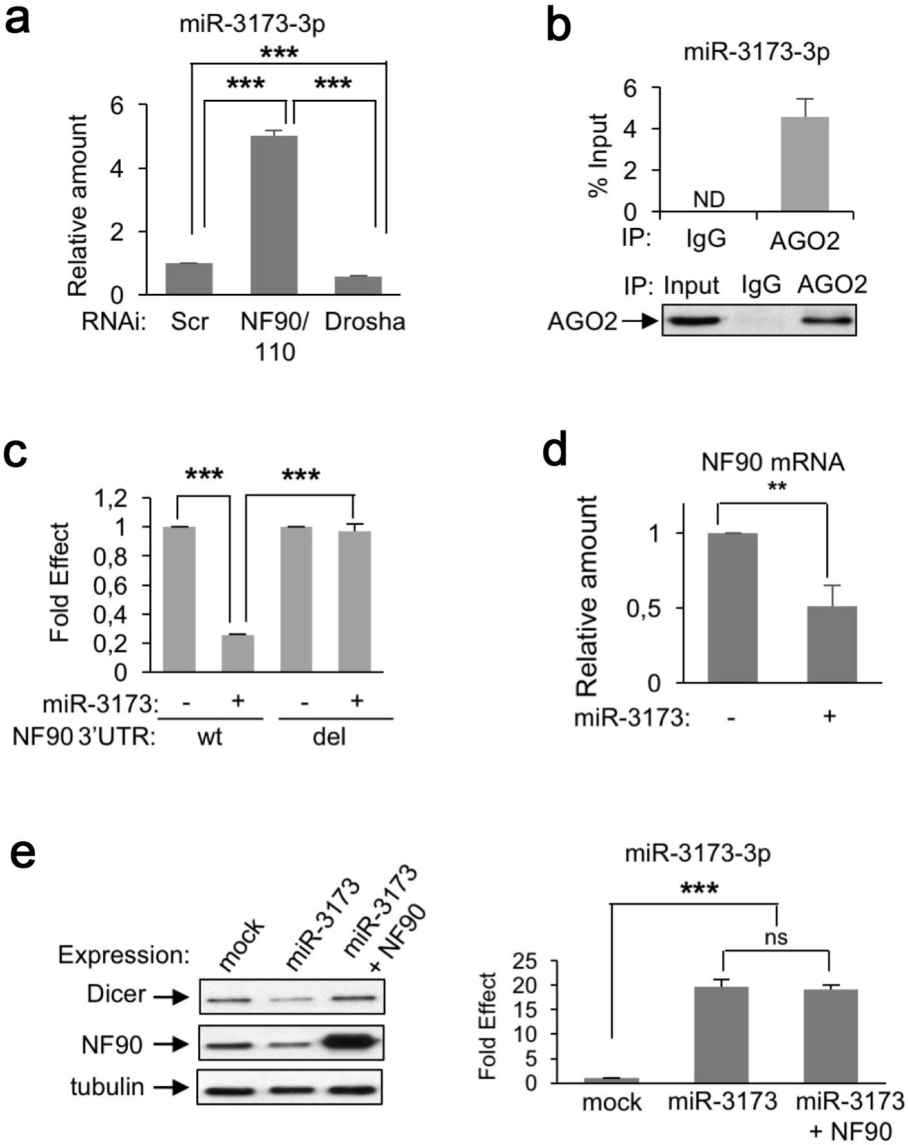

Fig. 3 MiR-3173-3p targets NF90 establishing a feedback amplification loop to control DICER expression. **a** N90/NF110 and Microprocessor inversely affect the abundance of miR-3173-3p. Extracts of 293T cells transfected with DROSHA- or NF90/NF110-specific siRNA or a non-targeting control were analyzed for the abundance of miR-3173-3p using Taqman RT-qPCR. Results were normalized by those obtained for U6 abundance in the same samples. Data represent mean ± SEM obtained from three independent experiments (***$P < 0.001$, independent Student's *t*-test). **b** MiR-3173 associates with Ago2. Extracts of 293T cells were immunoprecipitated with mock or anti-AGO2 antibody as indicated. Immunoprecipitates were analyzed using Taqman RT-qPCR for miR-3173-3p. Data represent mean ± SEM obtained from three independent experiments. ND indicates 'not detected'. **c** MiR-3173 targets NF90 3′-UTR. Extracts of 293T cells transfected with pMirGLO containing a region of NF90 3′-UTR (nt 3361–3476) either wild-type (WT) or deleted at the site targeted by miR-3173 (del) in the presence and absence of plasmid expressing miR-3173 as indicated, were analyzed by dual luciferase assay. Values for luciferase activity were normalized to those obtained for Renilla in the same samples. Data represent mean ± SEM obtained from three independent experiments (***$P < 0.001$, independent Student's *t* test). **d** Extracts of 293T cells transfected with miR-3173 or a control plasmid were analyzed by RT-qPCR for the abundance of NF90 mRNA. Results were normalized by those obtained for $tRNA^{lys}$ abundance in the same samples. Data represent mean ± SEM obtained from three independent experiments, **$P < 0.01$, independent Student's *t*-test). **e** MiR-3173 targets endogenous NF90 and diminishes DICER expression. Extracts of 293T cells transfected with plasmid expressing miR-3173, alone or together with a plasmid expressing NF90, or a mock control were analyzed by immunoblot using the indicated antibodies (left panel). Extracts were analyzed using Taqman RT-qPCR for miR-3173-3p (right panel). Results were normalized by those obtained for U6 abundance in the same samples. Data represent mean ± SEM obtained from three independent experiments (***$P < 0.001$, ns indicates not significant, independent Student's *t*-test)

associates with miR-3173 stem loop by carrying out RNA immunoprecipitation (RIP) using an anti-NF90 antibody followed by RT-qPCR. We found that NF90 was associated with the region containing miR-3173 but not with a downstream region (Fig. 2c). To obtain further insights into how Microprocessor and NF90/NF110 affect DICER pre-mRNA processing, we performed RIP analysis for these factors under conditions that affect splicing efficiency. Association of DROSHA with the region surrounding miR-3173 was not detectable in comparison with an experiment with mock samples in control (siScr) cells but was significantly enhanced following RNAi that diminished association of NF90 (Fig. 2d).

These data suggest that NF90/NF110 may modulate recruitment of Microprocessor by competing for association with pri-

miR-3173. To directly test this idea, we performed RNA electrophoretic mobility shift assay (RNA EMSA) using recombinant NF90 and the dsRNA-binding domains of DGCR8 (amino acids 484–773) (Supplementary information, Figure S2F) and the region of DICER pre-mRNA surrounding pre-miR-3173. RNA EMSA showed that addition of rNF90 resulted in band shifts, indicating the formation of rNF90-pri-miR-3173 complexes (Fig. 2e, compare lanes 1 and 2). Addition of antibody against NF90, but not mock IgG, resulted in the formation of super-shifted complexes (Fig. 2e, compare lanes 3 and 4 to lanes 5 and 6, super-shift) indicating that the shifted bands seen in lane 2 are rNF90-pri-miR-3173 complexes. Additionally, rNF90 bound more efficiently to pri-miR-3173 than to pri-miR-21, for which NF90 has a low affinity[35] (Supplementary information, Figure S2G, compare lanes 1–4 with lanes 5–8). We next tested whether rNF90 competes with DGCR8 for binding to pri-miR-3173. As expected, rDGCR8-dsRBDs formed a complex with pri-miR-3173 (Fig. 2f, lane 2). Interestingly, titration with rNF90 diminished the rDGCR8-dsRBDs/pri-miR-3173 complex, which was replaced by the rNF90/pri-miR-3173 complex, even at lower concentrations of rNF90 (0.6–4.8 μM) than rDGCR8-dsRBDs (4.8 μM) (Fig. 2f, compare lane 2 with lanes 3–6). This finding suggests that NF90 would preferentially bind to pri-miR-3173, even in the presence of Drosha-DGCR8.

In the absence of NF90/NF110, cropping of pri-miR-3173 by Microprocessor would therefore be predicted to result in cleavage of DICER pre-mRNA. To test this idea, modified 5′ RNA Ligase-Mediated (RLM)-Rapid Amplification of cDNA Ends (RACE) was performed as described previously.[42] In this analysis, a PCR product can be amplified only under conditions in which DICER pre-mRNA has been cleaved (Fig. 2g, schematic). Extracts of cells knocked-down for NF90/NF110 were highly permissive for amplification of the cleavage-specific PCR products compared with control (Scr) cells (Fig. 2g). Sequencing of the PCR products revealed that the cleavage occurred near the base of pri-miR-3173 stem loop that is the predicted Microprocessor cleavage site (Supplementary information, Figure S2H). These results suggest that NF90/NF110 suppresses cleavage of DICER pre-mRNA in the vicinity of miR-3173. Taken together, the findings suggest that, depending on their relative abundance, either Microprocessor or NF90 complexes associate with pri-miR-3173, which is embedded within intron 1 of DICER, to control splicing efficiency and consequently, DICER expression.

MiR-3173-3p targets NF90 establishing a feedback amplification loop to control DICER expression

We next wondered how NF90/NF110 and Microprocessor affect the processing of miR-3173 that is located within DICER intron 1. Knock-down of DROSHA reduced the abundance of mature miR-3173-3p by approximately twofold, whereas knock-down of NF90/NF110 increased its abundance by more than fivefold (Fig. 3a and Supplementary information, Figure S3A). In contrast, the abundance of Let-7a, measured in the same extracts, was diminished by loss of Drosha as expected but, unlike miR-3173-3p, was not increased by loss of NF90/NF110 under the conditions used in these experiments (Supplementary information, Figure S3B). Microprocessor therefore diminishes splicing and expression of DICER but promotes miR-3173 processing. Conversely, NF90/NF110 enhances DICER splicing and expression and reduces miR-3173 processing. Thus, the abundance of miR-3173-3p can be modulated inversely by Microprocessor and NF90/NF110.

To date, no mRNA targets of miR-3173-3p have yet been identified. We determined that miR-3173 is incorporated into RISC by performing immunoprecipitation of endogenous AGO2, followed by TaqMan qPCR for detection of miR-3173-3p (Fig. 3b), suggesting that miR-3173-3p may target one or more cellular mRNAs. We noted that the 3′-UTR of NF90 mRNA contains a consensus site that is predicted to bind miR-3173-3p (MiRDB).[43] We therefore tested the effect of miR-3173 expression on luciferase activity of pmirGlo containing a region of the 3′-UTR of NF90 wt sequence or in which the predicted target site for miR-3173-3p had been deleted (del). Figure 3c shows that miR-3173 diminishes luciferase activity from the WT 3′-UTR by approximately fourfold, whereas deletion of the miR-3173 target site relieved miR-3173-dependent repression. Expression of miR-3173 diminished the abundance of endogenous NF90 mRNA (Fig. 3d) and protein (Fig. 3e). Strikingly, the abundance of DICER was concomitantly reduced by miR-3173, but could be restored by co-expression of NF90 (Fig. 3e), which accords with the notion that NF90 modulates DICER expression.

MiR-3173-3p is conserved among certain primates, including chimpanzee, gorilla, green monkey, and macaque (Supplementary information, Figure S4A). Among primates that contain miR-3173-3p, the cognate binding site for miR-3173-3p is also present in the 3′-UTR of NF90 in these same species (Supplementary information, Figure S4B). Interestingly, the target site for miR-3173-3p can also be identified in some primates, such as marmoset, tarsier, and galago, which do not contain miR-3173-3p, whereas the target site for miR-3173-3p is not conserved outside the primate lineage (Supplementary information, Figure S4C). Thus, these data indicate that miR-3173-3p is conserved among certain primates and could potentially target NF90 mRNA in, for example, Old World monkeys.

The modulation of DICER expression by NF90/NF110 would be expected to deregulate the abundance of cellular miRNAs. This led us to perform miRNA profiling under conditions in which expression of either DICER or NF90/NF110 had been diminished. To this end, we isolated small RNAs between 18 and 26 nt in length from extracts of cells knocked-down for either DICER or NF90/NF110 and analyzed them by high-throughput sequencing. The increase in miR-3173-3p expression in NF90/NF110 knock-down cells was confirmed by small RNA-seq (Supplementary information, Figure S5). The alignment of reads mapping to miR-3173 furthermore showed a pattern typical of a miRNA, rather than a degradation product (Supplementary information, Figure S5), in support of the notion that miR-3173 is indeed a functional miRNA. Among the miRNAs that were downregulated, we found a significant overlap between miRNAs for which the expression decreased following loss of either DICER or NF90/NF110 ($P = 0.019$; hypergeometric test; Supplementary information, Table S1).

The ensemble of results show that NF90/NF110 regulates the processing of miR-3173, and that miR-3173 in turn targets NF90. Taken together, these results indicate that a feedback amplification loop is established that controls DICER expression and affects miRNA abundance.

Control of DICER expression by NF90 is mediated through pri-miR-3173

Low expression of DICER is an indicator of advanced tumor stage and poor clinical outcome among patients with solid tumors such as ovarian carcinoma.[26,27] We therefore wondered whether the feedback loop controlling DICER expression is relevant in ovarian carcinoma cells. The ovarian carcinoma cell lines, HO8910 and SK-OV-3, were selected for further study in parallel with a cell line obtained from patient-derived serous ovarian cancer xenograft (PDX), OVA2-BUR. Stable expression of NF90 in HO8910 and SK-OV-3 cells and OVA2-BUR PDX increased expression of endogenous DICER (Fig. 4a, b). Loss of NF90/110 in SK-OV-3 cells led to diminution of DICER expression, and concomitant increase in expression of miR-3173-3p (Supplementary information, Figure S6A). Taken together, these data suggest that NF90-mediated regulation can be used to modulate DICER expression in ovarian carcinoma cells.

The data obtained so far suggest that the occurrence of miR-3173 stem loop within DICER pre-mRNA is central to the regulation of DICER by NF90/NF110. We would expect that

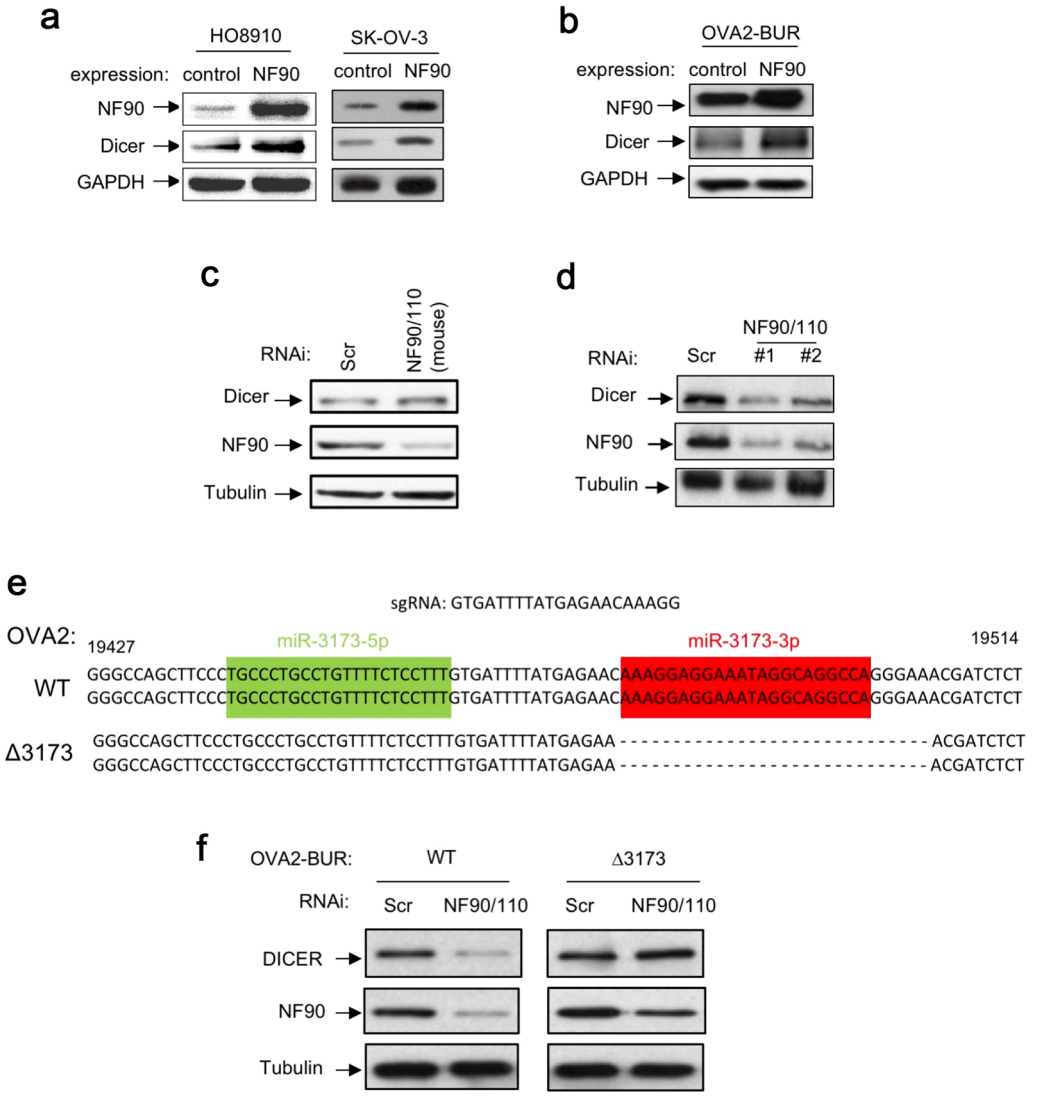

Fig. 4 Control of DICER expression by NF90 is mediated through miR-3173. **a**, **b** Overexpression of NF90 enhances DICER expression in ovarian cancer cells. Immunoblot analysis showing expression of NF90 and DICER in HO8910 cells (left panel) or SK-OV-3 cells (right panel) **a** or OVA2-BUR PDX **b** transduced with a lentivirus-expressing NF90 or an empty control as indicated on the figure. Expression of GAPDH was used as a loading control. **c** Extracts of NIH3T3 cells transfected with murine NF90/NF110-specific siRNA or a non-targeting control were analyzed by immunoblot using the indicated antibodies. **d** Extracts of OVA2-BUR PDX transfected with control or NF90/NF110-specific siRNAs as indicated were analyzed by immunoblot using the antibodies indicated. **e** Alignment of sequences corresponding to the genomic region containing pre-miR-3173 amplified from parental OVA2-BUR and OVA2-BURΔ3173. Numbers in nt refer to the position in the pre-mRNA sequence. Green- and red-shaded regions indicate the sequences of mature miR-3173-5p and -3p, respectively. The sequence of the sgRNA used for genome editing is shown above. **f** Extracts of OVA2-BUR or OVA2-BURΔ3173 transfected with control or NF90/NF110-specifc siRNA as indicated were analyzed by immunoblot using antibodies against DICER, NF90, and Tubulin, as indicated

absence of the stem loop structure would abolish NF90/NF110-mediated modulation of DICER. Indeed, DICER expression is not affected by NF90 in mouse cells that do not contain any annotated stem loop within DICER pre-mRNA (Fig. 4c). To address this in ovarian cancer cells, we employed OVA2-BUR cells because they express very low amounts of miR-3173 under control conditions (Supplementary information, Figure S6B). Upon loss of NF90/NF110, however, DICER expression in OVA2-BUR is strongly downregulated (Fig. 4d). These results support the idea that the miR-3173 stem loop within Dicer pre-mRNA plays a crucial role in the regulation of Dicer by NF90/NF110 in ovarian carcinoma cells. To further demonstrate this idea, the miR-3173 stem loop structure was partially deleted in OVA2-BUR using CRISPR-Cas9 genome editing (OVA2-BURΔ3173, Fig. 4e, Supplementary information, Figure S6B). Deletion of the miR-3173 stem loop structure modestly enhanced expression of DICER and NF90 under control conditions and knock-down of NF90 was less efficient in OVA2-BURΔ3173 compared with parental cells (Fig. 4f and Supplementary information, Figure S6C and D). This expected outcome may be due at least in part to loss of the feedback amplification loop controlling NF90 expression. Strikingly though, loss of NF90/NF110 no longer affected DICER expression in OVA2-BURΔ3173 that do not contain the stem loop structure. This contrasts to WT OVA2-BUR cells that contain the miR-3173 stem loop, in which a fivefold reduction in DICER expression was measured (Fig. 4f and Supplementary information, Figure S6D). Together, these findings suggest that NF90/NF110 controls DICER expression in ovarian cancer cells, in a manner that is influenced by the presence of the miR-3173 stem loop structure within DICER pre-mRNA.

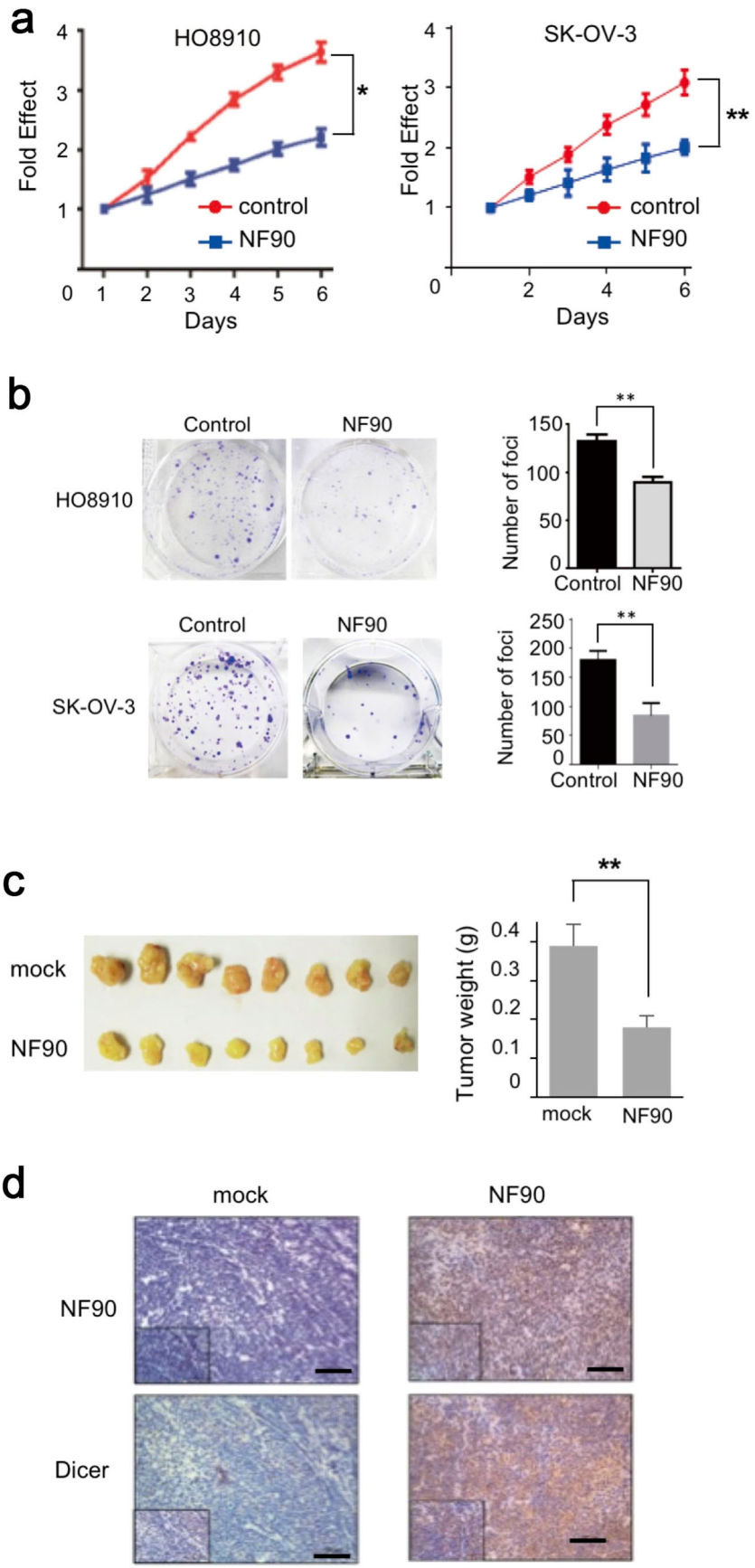
a
HO8910
SK-OV-3
Fold Effect
Days
control
NF90
*
**
b
Control
NF90
HO8910
SK-OV-3
Number of foci
c
mock
NF90
Tumor weight (g)
d
mock
NF90
Dicer

Fig. 5 NF90/NF110-dependent modulation of DICER expression controls proliferation of ovarian cancer cells in vitro and in vivo. **a** Growth rate of HO8910 (left panel) and SK-OV-3 cells (right panel) transduced with NF90-expressing or empty lentivirus, as indicated. Data are expressed as mean ± SD of three independent experiments (*$P < 0.05$, **$P < 0.01$, independent Student's *t*-test). **b** Representative images of colony foci formation in a monolayer culture of control or NF90-overexpressing HO8910 and SK-OV-3 cells. Quantitative analysis of foci numbers is shown in the adjacent graphs. Data are expressed as mean ± SD of three independent experiments (**$P < 0.01$, independent Student's *t*-test). **c** Image of the xenograft tumors formed in Balb/c nude mice injected with HO8910 cells infected with empty or NF90-expressing lentivirus as indicated. Weights of xenograft tumors are shown in the right panel. Data are shown as mean ± SD (**$P < 0.01$, independent Student's *t*-test). **d** Representative IHC images of NF90 and DICER expression in xenograft tumors of HO8910 cells (bar represents 100 μM)

NF90 shows tumor-suppressor activity in ovarian carcinoma cells in vivo

In ovarian carcinoma patients, low levels of DICER are associated with aggressive invasive disease and poor survival.[26,27] Thus, it is important to determine whether NF90-mediated regulation of DICER has an impact upon ovarian cancer cell growth and metastasis. NF90-dependent modulation of DICER was further analyzed in two ovarian carcinoma cell lines, HO8910 and SK-OV-3. Overexpression of NF90 reduced the proliferation of ovarian carcinoma cells (Fig. 5a and Supplementary information, Figure S6E) and a colony formation assay revealed that overexpression of NF90 also inhibited the number of cell foci (Fig. 5b). To determine whether NF90/NF110-dependent DICER regulation might affect tumor development in vivo, a subcutaneous xenograft tumor mouse model was established. Tumors derived from HO8910 cells ectopically expressing NF90 were reduced in size and weight compared with tumors from control cells (Fig. 5c). Immunohistochemistry (IHC) analysis of sections of HO8910 xenograft tumors confirmed the overexpression of NF90 and furthermore revealed concomitant elevated expression of DICER (Fig. 5d). Thus, modulation of NF90 expression in ovarian cancer cells affects cell proliferation rate and tumor development in vivo.

We next investigated the impact of NF90 on cell migration and invasion in ovarian carcinoma. Overexpression of NF90 in HO8910 and SK-OV-3 cells markedly diminished cellular invasion, as demonstrated by transwell invasion assays (Fig. 6a, b). To evaluate the role of NF90 on tumor metastasis in vivo, mice (six per group) were injected intravenously in the tail vein with HO8910 cells that had been infected with either empty or NF90-expressing lentivirus. After 4 weeks, the mice were sacrificed and the metastatic nodules in the lung were counted. Compared with those injected with control cells, mice injected with NF90-overexpressing cells had significantly less metastatic nodules in the lung (Fig. 6c, d). Hematoxylin and eosin (H&E) staining confirmed that the nodules were metastatic tumors (Fig. 6e). Thus, NF90 inhibits invasion and metastasis of ovarian carcinoma.

As miR-3173 targets NF90, which in turn diminishes the expression of DICER (Fig. 3c–e), we next investigated the impact of miR-3173 on cell invasion and tumor metastasis. We first confirmed that overexpression of miR-3173 diminished expression of NF90 and DICER in HO8910 and SK-OV-3 cells (Supplementary information, Figure S7A-B). Overexpression of miR-3173 significantly increased the invasiveness of ovarian carcinoma cells (Fig. 6f, g, miR-3173 panels). In vivo, significantly more metastatic nodules were induced at the surface of the lungs of mice injected with miR-3173-expressing HO8910 cells compared with the control (Fig. 6h–j, miR-3173 panels). To address whether miR-3173 promotes tumor invasion and metastasis through regulation of NF90, NF90 was overexpressed together with miR-3173 in ovarian carcinoma cells (Supplementary information, Figure S7A-B). Transwell assays showed that overexpression of NF90 counteracted the increased invasiveness of miR-3173-expressing HO8910 and SK-OV-3 cells (Fig. 6f, g, miR-3173 + NF90 panels). Similarly, in mice injected with miR-3173-expressing cells, the increased formation of metastatic nodules was reversed by co-overexpression of NF90 (Fig. 6h, i and Supplementary information, Figure S7C, miR-3173 + NF90 panels). Finally, to determine whether the effects of miR-3173 and NF90 on tumor invasion and metastasis were mediated through DICER, the reversal of these phenotypes observed after overexpression of NF90 was counteracted by expression of a short hairpin RNA (shRNA) targeting DICER (Fig. 6f, g, and Supplementary information, Figure S7A-C, far right panels). The expression level of NF90 and DICER in metastatic nodules was analyzed by IHC (Fig. 6k, l and Supplementary information, Figure S7D-E). Low expression of NF90 and DICER was associated with a high occurrence of metastasis. These data provide evidence that NF90 inhibits metastasis of ovarian carcinoma.

Clinical significance of NF90 expression in ovarian carcinoma patients

We next asked whether NF90 expression correlates with the clinicopathological status of patients with ovarian carcinoma. Kaplan–Meier analysis of 566 ovarian carcinoma samples from TCGA showed that low expression of NF90, like that of DICER, was associated with poor survival (Fig. 7a). In addition, a cohort of 169 ovarian carcinoma patient samples from China was statistically analyzed. The representativeness of the ovarian carcinoma patient population in the cohort was confirmed by analysis of established prognostic predictors of patient survival. Clinical parameters of pathology, such as tumor histological grade ($P = 0.02$), pT status ($P = 0.005$), pN status ($P < 0.001$), pM status ($P < 0.001$), and FIGO stage ($P < 0.001$), showed a statistically significant impact on patient survival (Supplementary information, Table S2). The expression level of NF90 in the ovarian carcinoma cohort samples was determined by X-tile[44] analysis. The cutoff point for high expression of NF90 was defined when H scores were above 40 (Supplementary information, Figure S8A-B). Among the cohort samples, low expression of NF90 was observed in 99 out of the 169 primary ovarian cancer tissues analyzed (58.57%) and was also associated with poor survival ($P < 0.001$) (Supplementary information, Table S2 and Figure S8C).

We next analyzed the association of NF90 expression with prognostic predictors of patient survival. As shown in Supplementary information, Table S3, low NF90 expression was positively associated with the histological tumor grade ($P = 0.015$), pN status ($P = 0.017$), pM status ($P = 0.001$) and FIGO stage of ovarian carcinomas ($P < 0.001$). Notably, >90% of FIGO stage IV patients showed low NF90 expression compared with only 36% of stage I patients (Supplementary information, Table S3).

We wondered whether or not the expression of NF90 protein and other clinical pathological parameters, such as tumor histological grade, pT/pN/pM status, and FIGO stage, might also significantly impact patient survival in multivariate analysis. Multivariate Cox regression analysis evaluated that NF90 expression, together with pN status ($P = 0.014$) and FIGO stage ($P = 0.018$), is an independent prognostic factor for adverse overall survival in ovarian carcinoma patients (relative risk: 0.508, confidence interval (CI): 0.269-0.959, $P = 0.037$, Supplementary information, Table S2). The mean disease-free survival time for low NF90-expressing ovarian carcinoma patients was 59.6 months compared with a survival time of 108.6 months for patients with

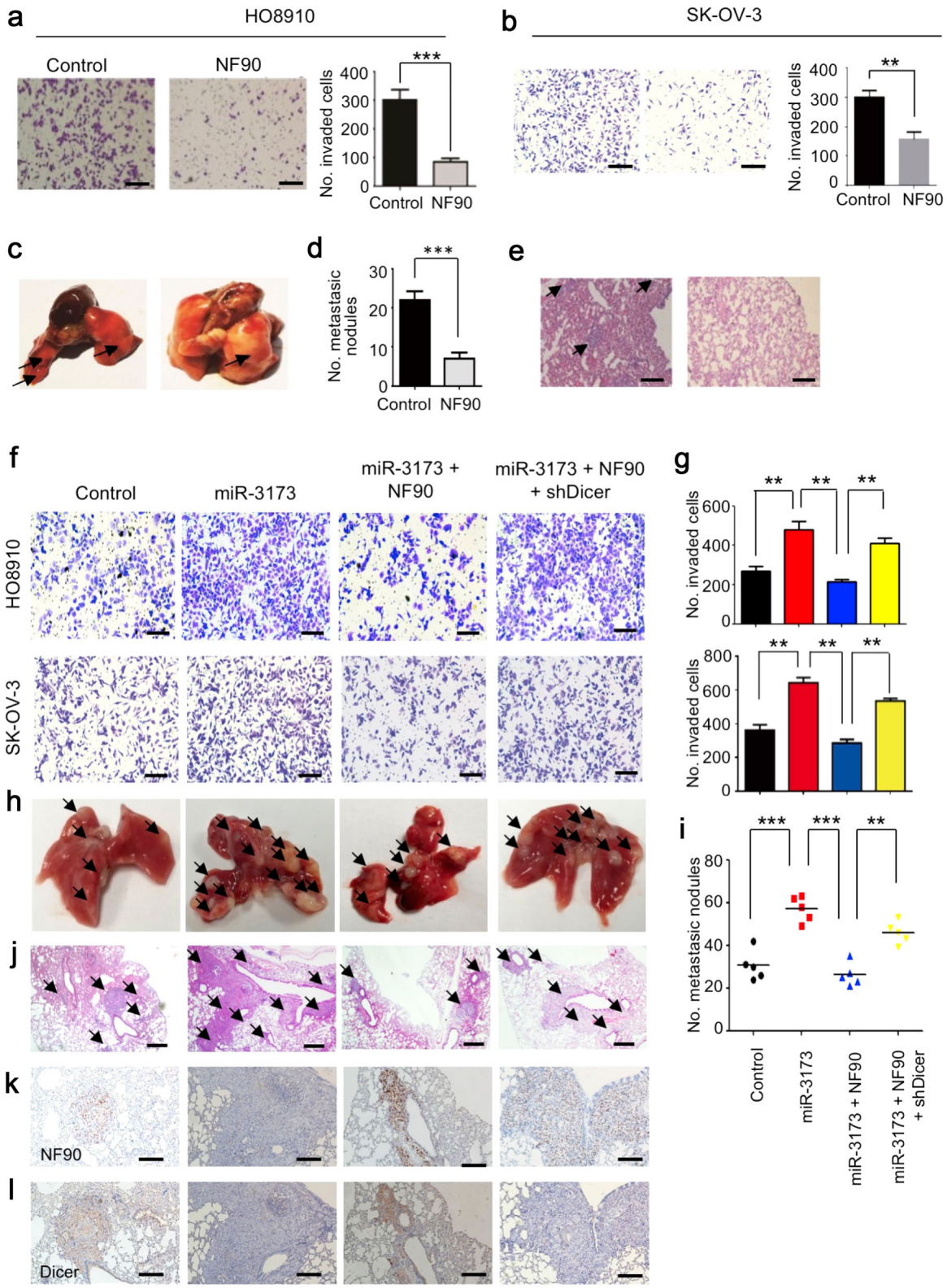

high expression levels of NF90 ($P < 0.001$, Fig. 7b and Supplementary information, Table S2).

In the final part of the present study, we further examined the correlation between the expression levels of NF90 and DICER in a cohort of 566 ovarian carcinomas from the TCGA database and in our cohort of 169 ovarian carcinomas. We found that the expression levels of DICER were positively correlated with that of NF90 in both cohorts ($P = 1e\text{-}05$, Fig. 7c and $P < 0.001$,

Fig. 6 NF90 inhibits ovarian cancer cell motility and metastasis in vivo. **a**, **b** NF90 inhibits cell invasion. HO8910 **a** and SK-OV-3 cells **b** infected with empty or NF90-expressing lentiviral vector, as indicated, were analyzed by transwell invasion assay. Representative images of invaded cells are shown in left panels (bar represents 100 μM). Results of transwell assays expressed as mean ± SD of three independent experiments (***$P < 0.001$, **$P < 0.01$, independent Student's *t*-test) are shown in right panels. **c**–**e** NF90 inhibits metastasis of ovarian cancer. Nude mice were injected in the tail vein with HO8910 cells, which had been transduced with empty or NF90-expressing lentivirus, as indicated. Representative images of lungs derived from mice injected with control of NF90-expressing cells are shown in **c**. Metastatic nodules at the surface of lungs are indicated by arrows. Numbers of metastatic nodules at the lung surfaces are expressed as mean ± SD of three independent experiments (***$P < 0.001$, independent Student's *t*-test) are shown in **d**. Representative images of H&E-stained sections derived from the lung metastatic nodules shown in **c** are shown in **e** (bar represents 100 μM). **f**–**l** Targeting of NF90 by miR-3173 controls tumor metastasis. HO8910 and SK-OV-3 **f**, **g** ovarian carcinoma cells transduced with lentiviruses expressing miR-3173, either alone or together with those expressing NF90 or shRNA targeting Dicer, as indicated, were analyzed by transwell invasion assay. Representative images of invaded cells are shown in **f** (bar represents 100 μM). Results of transwell assays, expressed as the mean ± SD obtained from three independent experiments (**$P < 0.01$, independent Student's *t*-test) are shown in **g**. Representative images of metastatic nodules on the surface of the lungs (indicated by arrows) derived from nude mice injected into the tail vein with HO8910 cells are shown in **h**. Consecutive tissue sections (112–153 sections) were made from each lung of mice and stained with hematoxylin-eosin (H&E) and the numbers of the pulmonary metastatic nodules were then carefully examined and counted under a microscope. Numbers of the metastatic nodules in the lungs of each group are shown in **i** (expressed as mean ± SD of three independent experiments, ***$P < 0.001$, **$P < 0.01$, independent Student's *t*-test). Representative images of H&E staining of metastatic carcinoma lesions in the lungs examined under the microscope are shown in **j** (bar represents 400 μM). Representative IHC images showing expression of NF90 (shown in **k**) and DICER (shown in **l**), in which the expression levels of NP90 and DICER were scored in a semiquantitative count method by evaluating the number of positive carcinoma cells over the total number of carcinoma cells. NF90 expression: 70%, 0%, 90%, 80% (from left to right of different treated conditions); DICER expression: 60%, 0%, 80%, 0% (from left to right of different treated conditions). Bar represents 200 μM

Supplementary information, Table S3). Moreover, we revealed that the expression levels of miR-3173-3p had a significantly negative correlation with that of either Dicer ($P = 0.001$) or NF90 expression ($P = 0.003$, Fig. 7d), and furthermore, high expression of miR-3173 was evaluated to predict the poorest survival of ovarian carcinoma patients ($P < 0.001$, Fig. 7e). These data, together with our findings in ovarian carcinoma cell lines, provided further evidence that in ovarian carcinoma, expression of Dicer might be mediated by NF90 through miR-3173.

DISCUSSION

We report here an NF90/NF110-mediated feedback amplification loop that regulates DICER expression to control ovarian tumor progression and metastasis (Fig. 8). We show that a miRNA, miR-3173, which is embedded in the first intron of DICER pre-mRNA acts as a control point enabling NF90/NF110 to modulate DICER expression by inhibiting access to Microprocessor. Association of NF90/NF110 diminishes pri-miR-3173 cropping, enhances splicing efficiency and, consequently, increases DICER expression. Low expression of NF90/NF110 on the other hand leads to cleavage of DICER pre-mRNA by Microprocessor, resulting in low expression of DICER. As the control point, miR-3173, in turn targets NF90, a feedback amplification loop is established that controls DICER expression. Thus, small changes in NF90/NF110 abundance could be amplified by the feedback loop to create significant changes in DICER expression.

Interestingly, miR-3173-3p is conserved among certain primates (chimpanzee, gorilla, green monkey, and macaque) but is not present in other species. Furthermore, the cognate binding site for miR-3173-3p is present in the 3′-UTR of NF90 in these same species, as well as the marmoset, tarsier, and galago, which do not contain miR-3173-3p (Supplementary information, Figure S4). In contrast, neither miR-3173-3p nor its cognate binding site are present in mouse. Dicer transcripts from other species do not contain any other annotated hairpin structures, with the exception of *Arabidopsis thaliana*, which contains an annotated miRNA (miR-838a) within one of its Dicer isoforms. Interestingly, miR-838a is also localized within a long intron and is present only in the isoform required for miRNA biogenesis (Dicer-like-1). It is, however, not known whether modulation of DICER expression through Microprocessor/NF90 and miR-3173 also occurs in other primates and if a similar mechanism also occurs in *A. thaliana*.

Processing of miRNAs has been shown to occur co-transcriptionally.[38,39,45] As the majority of human miRNAs are localized in introns, their processing could potentially interfere with splicing. However, previous studies have shown that the cropping of certain intron-embedded miRNAs, such as miR-26A1 and miR-26B, did not significantly affect the splicing of the intron,[38,39] and we also confirmed these findings (Supplementary information, Figure S1F-G). However, unlike these miRNAs, cropping of miR-3173 embedded in the first intron of DICER was not compatible with splicing. It is currently unclear why these same processes may affect the outcome of gene expression differently. We note that the miRNA hosting introns whose splicing was not affected by cropping are much shorter than intron 1 of DICER, which is 25 kB in length. It is possible that the kinetics of splicing versus cropping may have a different impact on short versus long introns.

Ovarian cancer, which is the most prevalent gynecological cancer worldwide,[1,2] is associated with a high mortality rate. Only 30% of patients with advanced-stage disease survive >5 years after initial diagnosis.[4] Our findings reveal that the expression level of NF90 is an important factor in the progression and metastasis of ovarian carcinoma. Overexpression of NF90 significantly diminished tumor size, invasiveness, and metastasis in a xenograft mouse model. In TCGA and SYSUCC cohorts of ovarian carcinoma patients, low expression level of NF90 was associated with poor survival, worse pN/pM status, and advanced FIGO stage. Furthermore, the mean disease-free survival time for high NF90-expressing patients was almost double that of patients with low levels of NF90 (108.6 months compared with 59.6 months). Taken together, these data suggest that NF90 can act as a novel suppressor of ovarian carcinoma.

These findings have potential for novel therapeutic applications. NF90 expression level could be used as a prognostic marker for ovarian carcinoma progression. It would be instructive to perform longitudinal studies on ovarian carcinoma patients to determine whether expression of NF90 diminishes in parallel with advancing disease, or whether low NF90 expression from the outset could be used to predict patient groups that are likely to advance to late stage disease. Classification of patients based on NF90 expression could therefore influence therapeutic choices.

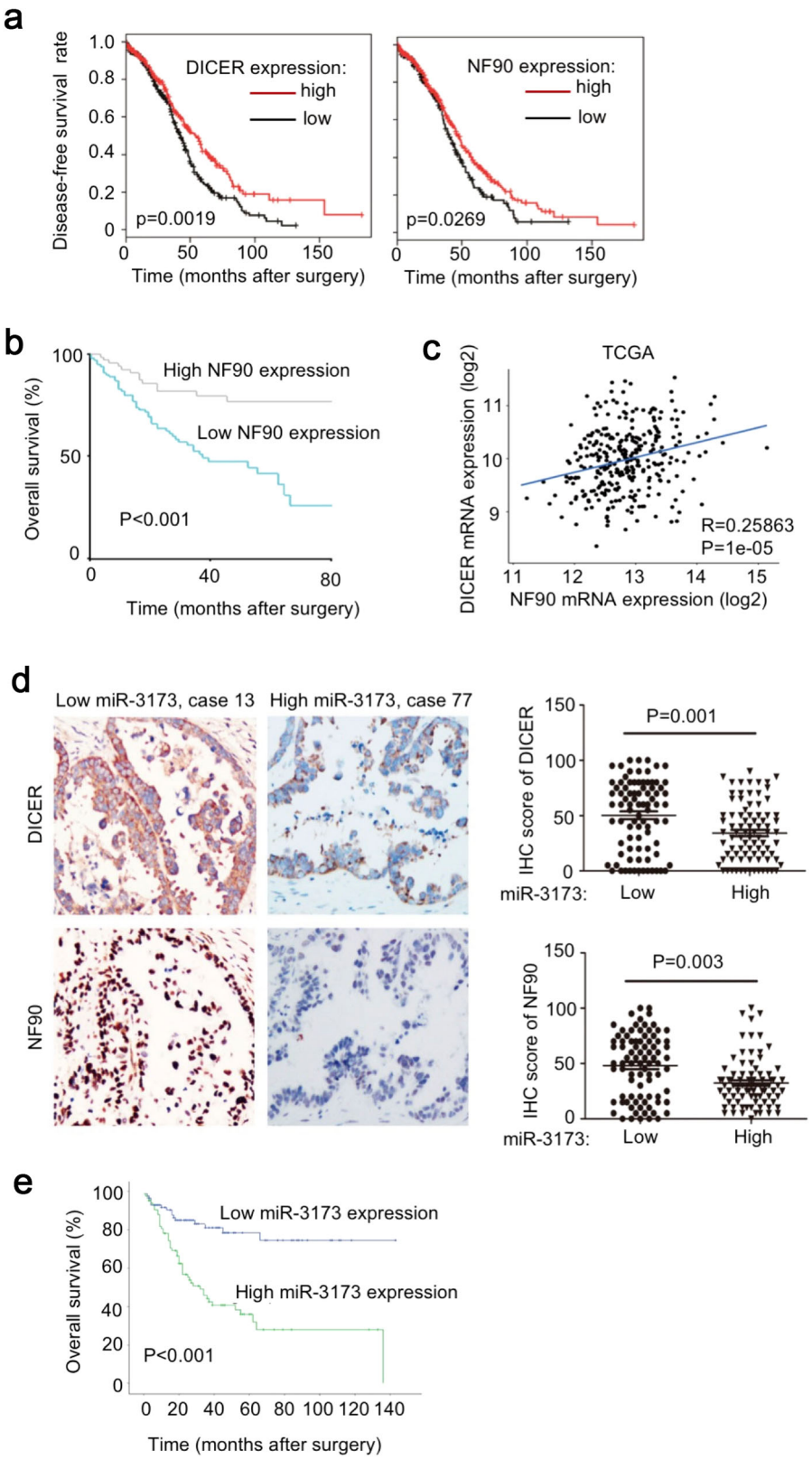

A major factor contributing to the high mortality rate of ovarian cancer is the lack of an early screening strategy. We found that overexpression of miR-3173 could induce metastasis in an NF90-dependent manner. Circulating cell-free miRNAs have been shown to enable earlier cancer diagnosis and to predict prognosis and response to therapy.[46] As miR-3173 is very poorly expressed in healthy cells due to high levels of NF90, the presence of circulating miR-3173 in patients' blood could potentially be used

Fig. 7 Low expression of NF90 or DICER predicts poor clinical outcome in patients with ovarian cancer. **a** Kaplan–Meier plot analysis of TCGA data indicates that low mRNA expression of DICER or NF90 is associated with poor prognosis of ovarian cancer patients ($P = 0.0019$ and $P = 0.0269$, respectively, by log-rank analysis, $n = 566$). **b** Kaplan–Meier plot analysis of data obtained from a Chinese cohort of ovarian cancer patients indicates that low NF90 expression is associated with poor prognosis ($P < 0.001$ by log-rank analysis). **c** Pearson correlation analysis demonstrates that the expression of NF90 is positively correlated with that of DICER ($R = 0.25863$; $P = 1e\text{-}05$) in ovarian carcinoma tissues from TCGA database. **d** Representative immunohistochemical staining of NF90 and DICER expression in two ovarian carcinoma cases, in which case 13 with low miR-3173-3p levels has high expression of both NF90 and DICER, and case 77 with high miR-3173-3p levels shows low expression of both NF90 and DICER (left panel). High levels of miR-3173-3p are correlated with low levels of NF90 and DICER in 169 cases of ovarian carcinoma FFPE tissues (right panels). Staining intensities for NF90 and DICER were significantly reduced ($P = 0.003$ and $P = 0.001$, respectively, by two-tailed Student *t*-test) in ovarian carcinomas with high miR-3173-3p compared with those with low miR-3173-3p. **e** Kaplan–Meier plot analysis of data obtained from a cohort of 169 ovarian carcinoma patients indicates that high expression of miR-3173-3p is associated with patients' poor prognosis ($P < 0.001$ by log-rank analysis)

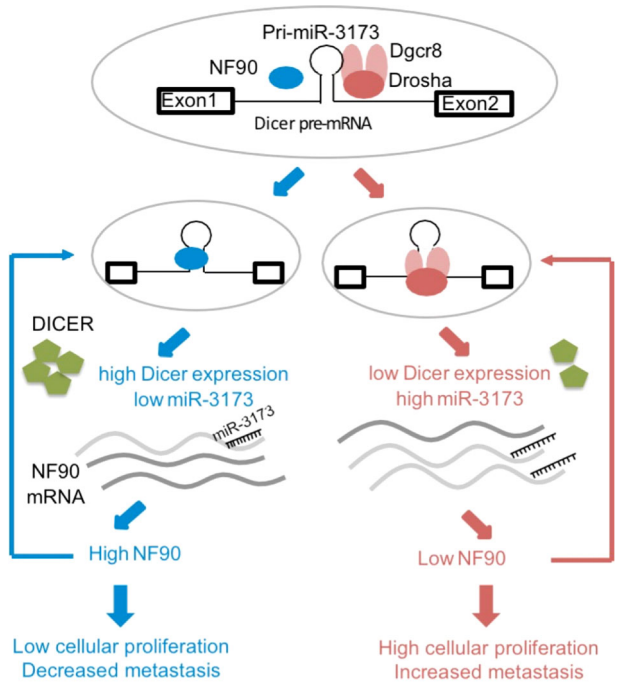

Fig. 8 A schematic showing a hypothetical model for the feedback regulation of DICER expression by Microprocessor and NF90 complexes. See text for details

as a biomarker of ovarian carcinoma. Thus, examination of circulating levels of miR-3173 might be exploited as a screening strategy that may detect ovarian carcinoma in patients prior to the onset of large-scale metastasis.

In summary, our findings have identified a novel regulatory mechanism of DICER expression that is mediated by NF90/NF110. This regulatory mechanism may play an important role in the progression of ovarian carcinomas. These findings open new possibilities for the development of approaches that can intervene in the NF90/NF110-mediated regulation of DICER. Such approaches could dramatically promote survival in patients with ovarian carcinoma.

MATERIALS AND METHODS

Antibodies and plasmids

Antibodies used in this study are listed in Supplementary information, Table S4. Plasmids encoding WT DROSHA and the mutant lacking endonucleolytic activity (E1045Q/E1222Q) have been described previously.[10] HA-Flag-NF90 was amplified from Flag-DRBP76[47] and cloned into pOZ for retroviral particle production. The 3′-UTR of NF90 (nt 3361–3476 of NF90 mRNA) was cloned into pMirGLO to generate pMirGLO-NF90 3′-UTR wt and was used as a template to generate pMirGLO-NF90 3′-UTR del in which the region complementary to miR-3173 seed region (nt 2–8) had been deleted. MiR-3173 was cloned into pGIPZ. A lentiviral vector psi-LVRH1H-expressing shRNA targeting Dicer was purchased from Genecopoeia.

Cell culture, treatment, transfection, and lentiviral infection

HeLa cells were propagated in Dulbecco's modified Eagle's medium (DMEM) supplemented with 10% fetal bovine serum (FBS) and antibiotics. 293T were grown in DMEM with Hepes (25 mM), supplemented with 10% FBS and antibiotics. Human ovarian carcinoma cell lines A2780, SKOV3, HO8910, COV504, ES2, and OVCAR3 were a gift from the First Affiliated Hospital of Sun Yat-sen University. SKOV3, HO8910, COV504, ES2, OVCAR3 were cultured in RPMI-1640 (Invitrogen) supplemented with 10% FBS. A2780 were cultured in DMEM supplemented with 10% fetal bovine serum. The OVA2-BUR patient-derived xenograft cell line was propagated in advanced DMEM/F12 supplemented with 10% FBS and antibiotics. All cells were grown in a humidified incubator at 37 °C with 5% CO_2.

Cells were transfected with siRNAs (30 nM final concentration) using Interferin (PolyPlus Transfection) according to the manufacturer's instructions. Plasmid transfection was performed with Jet PEI (PolyPlus Transfection) or Lipofectamine 3000 (Thermofisher Scientific) according to the manufacturer's instructions. All samples were harvested at approximately 60 h post-transfection. For virus infection, NF90-expressing lentivirus was produced and cells were infected as described previously.[48] The production of lentivirus-expressing shRNA against Dicer and infection of HO9810 and SK-OV-3 cells were performed using Lenti-Pac Kit from Genecopoeia according to the manufacturer's instructions.

siRNAs and QPCR oligonucleotides

Target sequences of dsRNA oligonucleotides used for RNAi (Eurofins MWG Operon or IDT) are shown in Supplementary information, Table S5. Sequences of PCR primers used in this study are shown in Supplementary information, Table S6.

Immunoblot and IHC analyses

For immunoblot, protein extracts were obtained using RIPA buffer (50 mM Tris-HCl pH = 7.5, 150 mM NaCl, 1% NP40, 0.5% sodium deoxycholate, 0.1% sodium dodecyl sulfate) supplemented with Complete protease inhibitor (Roche). Protein extracts were immunoblotted using the indicated primary antibodies (Supplementary information, Table S4) and anti-mouse or anti-rabbit IgG-linked horseradish peroxidase secondary antibodies (GE Healthcare) followed by ECL (ThermoFisher).

IHC studies were performed following a standard streptavidin–biotin–peroxidase complex method.[49] Tissue microarray (TMA) slides were incubated respectively with anti-NF90 (Santa Cruz, 1:400 dilution), Dicer (Abcam, 1:200 dilution). Immunostaining was performed using the Envision System with diaminobenzidine (Dako). A negative control was obtained by replacing the primary antibody with a normal IgG. Known

immunostaining positive cases were used as positive controls. The immunoreactivity for NF90 was scored in a semiquantitative method. In brief, each TMA spot was assigned an intensity score from 0 to 3 (I0, I1–3). The proportion of tumor cells of that intensity was then divided by the total number of tumor cells and recorded in 5% increments from 0 to 100 (P0, P1–3). The final H score (range 0–300) was determined by adding the sum of the scores obtained for each intensity and the proportion of the area stained (H score = [I1 × P1] + [I2 × P2] + [I3 × P3]). All histological evaluations were performed in a double-blind manner by two independent expert pathologists (Drs M. Cai and D. Xie). X-tile plots were used for assessment of NF90 expression and optimization of cut-point based on outcome.[44] The X-tile plots allowed determination of an optimal cutoff value while correcting for the use of minimum *P* statistics by Miller–Siegmund *P*-value correction.[44]

Quantitative RT-PCR

Total RNA was extracted from cells using TRIzol (ThermoFisher Scientific) according to the manufacturer's instructions. Extracts were treated with DNase I (Promega) and reverse transcribed using SuperScript III First-Strand Synthesis System (ThermoFisher Scientific). RT products were amplified by real-time PCR (Light-cycler, Roche) using Quanti Tect SYBR Green (Qiagen) with the indicated oligonucleotides. QPCR cycling conditions are available on request. Sequences of qPCR primers used in this study are shown in Supplementary information, Table S6. RT and qPCR of miR-3173-3p and Let-7a were performed by Taqman (Thermo-Fisher Scientific).

miRNA isolation and quantitative real-time polymerase chain reaction from FFPE specimens

Total RNA was extracted from ovarian carcinoma FFPE specimens with use of TRIzol reagent (Invitrogen, Carlsbad, CA, USA) as described previously.[50,51] Real-time polymerase chain reaction (RT-PCR) was carried out using SYBR Green SuperMix (Roche, Basel, Switzerland) to assess the prognostic value of miR-3173.[44] Relative expression of miR-3173 (fold normalized to U6) was classified into two groups (i.e., low expression and high expression) based on the median value of 2.16.

ChIP and RNA-ChIP

HEK293T cells were transfected as indicated in the figures. Following 64-h incubation, cells were washed and harvested for cross-link ChIP or RNA-ChIP, which were performed as described previously[52] using the antibodies indicated. Samples were amplified by qPCR or RT-qPCR using the primer pairs indicated. An aliquot of chromatin was amplified in parallel and values obtained for immunoprecipitates were normalized to values for chromatin (% input).

Modified 5′ RLM RACE and RNA EMSA

HEK293T cells were transfected as indicated in the figures. Following 64-h incubation, cells were washed and harvested for 5′ RLM RACE, which was performed according to the manufacturer's instructions (Life Technologies). PCRs were performed using the primers shown in Supplementary information, Table S6.

RNA EMSA was performed as described previously[35] using the recombinant proteins indicated on the figure. The pri-miR-3173 probe was amplified by PCR using the primers shown in Supplementary information, Table S6 and pri-miR-21 probe was synthesized as described previously.[35] Probes were re-annealed by heating to 95 °C for 5 min, 60 °C for 30 min, 42 °C for 60 min, followed by 20 °C for 15 min in a thermal cycler prior to use in EMSA. Anti-NF90 antibody used for super-shift assay has been described previously.[35]

CRISPR-Cas9 genome editing

MiR-3173 was partially deleted from OVA2-BUR PDX using CRISPR-Cas9 genome editing as described previously.[53] Guide sequences in DICER intron 1 (pre-mRNA 19,475 to 19,500, accession no. NM_177438) were selected using web-based prediction software, CHOPCHOP,[54] and cloned into pSpCas9(BB)-2A-GFP (PX458; Addgene plasmid # 48138).[53] Cells were transfected with Trans-IT (Mirus Bio). Disruption of miR-3173 was determined by PCR-based genotyping using the screening primers listed in Supplementary information, Table S6. Positive clones were further screened by Taqman RT-qPCR analysis for miR-3173-3p. Clone OVA2-BURΔ3173 was selected for further analysis.

miRNA profiling

HEK293T cells were transfected with control, Dicer- or NF90/NF110-specific siRNAs. Total RNA extracts were prepared 7-day post-transfection using TRIzol according to the manufacturer's instructions. Small RNA-seq was performed by Fasteris. Statistical analysis was performed using DESeq2.

Patients' and tissue specimens

A total of 169 cases of epithelial ovarian carcinomas were obtained from the archives of paraffin-embedded tissues between 1996 and 2008 at the Department of Pathology, Cancer Center and the First Affiliated Hospital, Sun Yat-sen University, Guangzhou, China. Data on survival time and clinical pathological parameters were also collected. All patients included in this study provided informed consent. Patients who had received complete resection and not received preoperative chemo-radiation therapy and had complete clinical follow-up data available for review were selected for this study. Patients who had incomplete clinical follow-up data or had died from unknown causes and emergencies were excluded. The use of clinical materials for research purposes was reviewed and approved by the Medical Ethical Committee of Sun Yat-sen University.

Construction of TMAs

The tissue microarray was constructed according to previously described methods.[55] Briefly, individual donor tissue block and matching histological H&E-stained slides were overlaid for tissue TMA sampling. The slides were reviewed by a senior pathologist, who marked representative areas of usable tumor tissues. The tissues were sampled with a tissue-arraying instrument (Beecher Instruments); 0.6-mm-diameter cylinder of tissue were selected in triplicate, removed from tumor areas of individual donor tissue block and re-embedded into a recipient paraffin block at the predetermined position. Subsequently, multiple sections (5 µm thick) were cut from the TMA block and mounted on microscopic slides.

Statistical analyses

In survival analysis, the optimal cut-point for expression of NF90 and miR-3173 was obtained using X-tile software version 3.6.1 (Yale University School of Medicine, New Haven, CT)[44] and median value of miR-3173 (i.e., 2.16), respectively. For univariate survival analysis, survival curves were obtained using the Kaplan–Meier method. The Cox proportional hazards regression model was performed for multivariate survival analysis. The correlation between NF90 expression and Dicer expression and clinicopathological features in ovarian carcinoma patients were analyzed using the chi-square test or Fisher's exact test. The independent Student's *t*-test was performed to analyze the statistical significance between two preselected groups. *P*-value of <0.05 was considered statistically significant.

Cell proliferation and oncogenic assays

For cell growth assays, cells were seeded in 96-well plates at a density of 1×10^3 cells per well, and cell growth rate was

assessed with the CCK8 kit (Dojindo Laboratory) or by MTT assay (Promega).

For foci formation assay, 2×10^2 cells were seeded in six-well plates, and after 2 weeks of culture cell colonies were counted by crystal violet staining. The transwell invasion assay was performed with BD BioCoat Matrigel Invasion Chambers (Becton Dickinson Labware, Franklin Lakes, NJ) following the manufacturer's instructions. The matrigel membrane was stained with crystal violet and migrated cells were counted under a microscope.

Xenograft tumor growth assay was established by subcutaneous injection of 5×10^6 cells, either control or ectopically expressing NF90, into the dorsal flank of 4-week-old Balb/c nude mice. Tumor formation was checked after 4 weeks. All animal experiments were conducted according to the institutional standard guidelines at Sun Yat-Sen University.

Experimental in vivo metastasis model

Eight 4-week-old Balb/c nude mice in each experimental group were injected with 1×10^6 cells, into the tail vein in a laminar flow cabinet. Four weeks after cell injection, mice were killed and examined. In vivo metastasis model, the lungs were removed and fixed with phosphate-buffered formalin. Subsequently, consecutive tissue sections (112–153 sections) were made for each block of the lung. Finally, total numbers of the pulmonary metastatic nodules in the lung were carefully examined and counted under microscope as previously described.[56,57]

ACKNOWLEDGEMENTS

We thank V.N. Kim for pFlag-DROSHA, C. Basler for pFlag-DRBP76, Feng Zhang for pSpCas9(BB)-2A-GFP (PX458; Addgene plasmid # 48138), and members of the labs for helpful discussions. J.B. and G.S. were supported by ANRS and ERC, X.C. by CNRS, FRM FDT20111223640 and NSFC, M.H. and P.G. by ERC and L.B. by FRM. This work was supported by grants from the National Key R&D Program of China (no. 2017YFC1309001 and no. 2016YFC1302305) to D.X., ARC SFI20121205660, FRM DEQ20130326505 and ING20121226264, MSDAvenir and ERC CoG RNAmedTGS to R.K., Japan Society for the Promotion of Science Grant-in-aid for Young Scientists (B) 17K15601, Grant-in-aid for Scientific Research (C) 16K08590 to S.S. and NSFC 81602233 to X.C.

AUTHOR CONTRIBUTIONS

J.B., X.C., G.S., M.C., X.Co., M.H., T.H., P.G., G.Y., Z.F., R.N.-S., W.R., S.R., O.D., L.B. and J.-G.J. conducted the experiments. J.B., G.S., X.C., S.S., D.X. and R.K. designed the experiments and D.X. and R.K. wrote the paper.

ADDITIONAL INFORMATION

Supplementary information accompanies this paper at https://doi.org/10.1038/s41422-018-0016-8.

Competing interests: The authors declare that they have no conflict of interest.

REFERENCES

1. Ferlay, J. et al. Cancer incidence and mortality worldwide: sources, methods and major patterns in GLOBOCAN 2012. *Int. J. Cancer* **136**, E359–E386 (2015).
2. Siegel, R. L., Miller, K. D. & Jemal, A. Cancer statistics, 2016. *CA Cancer J. Clin.* **66**, 7–30 (2016).
3. Bast, R. C. Jr., Hennessy, B. & Mills, G. B. The biology of ovarian cancer: new opportunities for translation. *Nat. Rev. Cancer* **9**, 415–428 (2009).
4. Jemal, A. et al. Cancer statistics, 2004. *CA Cancer J. Clin.* **54**, 8–29 (2004).
5. Naora, H. & Montell, D. J. Ovarian cancer metastasis: integrating insights from disparate model organisms. *Nat. Rev. Cancer* **5**, 355–366 (2005).
6. Buys, S. S. et al. Effect of screening on ovarian cancer mortality: the Prostate, Lung, Colorectal and Ovarian (PLCO) Cancer Screening Randomized Controlled Trial. *JAMA* **305**, 2295–2303 (2011).
7. Mei, L. et al. Maintenance chemotherapy for ovarian cancer. *Cochrane Database Syst. Rev.* CD007414 (2013).
8. Denli, A. M., Tops, B. B., Plasterk, R. H., Ketting, R. F. & Hannon, G. J. Processing of primary microRNAs by the Microprocessor complex. *Nature* **432**, 231–235 (2004).
9. Gregory, R. I. et al. The microprocessor complex mediates the genesis of microRNAs. *Nature* **432**, 235–240 (2004).
10. Han, J. et al. *The Drosha-DGCR8 compl*ex in primary microRNA processing. *Genes Dev.* **18**, 3016–3027 (2004).
11. Lee, Y. et al. The nuclear RNase III Drosha initiates microRNA processing. *Nature* **425**, 415–419 (2003).
12. Bernstein, E., Caudy, A. A., Hammond, S. M. & Hannon, G. J. Role for a bidentate ribonuclease in the initiation step of RNA interference. *Nature* **409**, 363–366 (2001).
13. Grishok, A. et al. Genes and mechanisms related to RNA interference regulate expression of the small temporal RNAs that control C. elegans developmental timing. *Cell* **106**, 23–34 (2001).
14. Ketting, R. F. et al. *Dicer functions in RNA* interference and in synthesis of small RNA involved in developmental timing in C. elegans. *Genes Dev.* **15**, 2654–2659 (2001).
15. Knight, S. W. & Bass, B. L. A role for the RNase III enzyme DCR-1 in RNA interference and germ line development in Caenorhabditis elegans. *Science* **293**, 2269–2271 (2001).
16. Ha, M. & Kim, V. N. Regulation of microRNA biogenesis. *Nat. Rev. Mol. Cell Biol.* **15**, 509–524 (2014).
17. Lin, S. & Gregory, R. I. MicroRNA biogenesis pathways in cancer. *Nat. Rev. Cancer* **15**, 321–333 (2015).
18. Lu, J. et al. MicroRNA expression profiles classify human cancers. *Nature* **435**, 834–838 (2005).
19. Kumar, M. S., Lu, J., Mercer, K. L., Golub, T. R. & Jacks, T. Impaired microRNA processing enhances cellular transformation and tumorigenesis. *Nat. Genet.* **39**, 673–677 (2007).
20. Kumar, M. S. et al. Dicer1 functions as a haploinsufficient tumor suppressor. *Genes Dev.* **23**, 2700–2704 (2009).
21. Martello, G. et al. A MicroRNA targeting dicer for metastasis control. *Cell* **141**, 1195–1207 (2010).
22. Melo, S. A. et al. A genetic defect in exportin-5 traps precursor microRNAs in the nucleus of cancer cells. *Cancer Cell* **18**, 303–315 (2010).
23. Su, X. et al. TAp63 suppresses metastasis through coordinate regulation of Dicer and miRNAs. *Nature* **467**, 986–990 (2010).
24. Grelier, G. et al. Prognostic value of Dicer expression in human breast cancers and association with the mesenchymal phenotype. *Br. J. Cancer* **101**, 673–683 (2009).
25. Karube, Y. et al. Reduced expression of Dicer associated with poor prognosis in lung cancer patients. *Cancer Sci.* **96**, 111–115 (2005).
26. Merritt, W. M. et al. Dicer, Drosha, and outcomes in patients with ovarian cancer. *N. Engl. J. Med.* **359**, 2641–2650 (2008).
27. Shan, W. et al. Role of Dicer as a prognostic predictor for survival in cancer patients: a systematic review with a meta-analysis. *Oncotarget* **7**, 72672–72684 (2016).
28. Jafarnejad, S. M., Ardekani, G. S., Ghaffari, M., Martinka, M. & Li, G. Sox4-mediated Dicer expression is critical for suppression of melanoma cell invasion. *Oncogene* **32**, 2131–2139 (2013).
29. Levy, C. et al. Lineage-specific transcriptional regulation of DICER by MITF in melanocytes. *Cell* **141**, 994–1005 (2010).
30. Yu, Z. et al. Cyclin D1 induction of Dicer governs microRNA processing and expression in breast cancer. *Nat. Commun.* **4**, 2812 (2013).
31. Feinberg-Gorenshtein, G. et al. MiR-192 directly binds and regulates Dicer1 expression in neuroblastoma. *PLoS One* **8**, e78713 (2013).
32. Forman, J. J., Legesse-Miller, A. & Coller, H. A. A search for conserved sequences in coding regions reveals that the let-7 microRNA targets Dicer within its coding sequence. *Proc. Natl. Acad. Sci. USA* **105**, 14879–14884 (2008).
33. van den Beucken, T. et al. Hypoxia promotes stem cell phenotypes and poor prognosis through epigenetic regulation of DICER. *Nat. Commun.* **5**, 5203 (2014).
34. Castella, S., Bernard, R., Corno, M., Fradin, A. & Larcher, J. C. Ilf3 and NF90 functions in RNA biology. *Wiley Interdiscip. Rev. RNA* **6**, 243–256 (2014).
35. Sakamoto, S. et al. The NF90-NF45 complex functions as a negative regulator in the microRNA processing pathway. *Mol. Cell. Biol.* **29**, 3754–3769 (2009).
36. Todaka, H. et al. Overexpression of NF90-NF45 represses myogenic microRNA biogenesis, resulting in development of skeletal muscle atrophy and centronuclear muscle fibers. *Mol. Cell. Biol.* **35**, 2295–2308 (2015).
37. Wagschal, A. et al. Microprocessor, Setx, Xrn2, and Rrp6 co-operate to induce premature termination of transcription by RNAPII. *Cell* **150**, 1147–1157 (2012).
38. Kim, Y. K. & Kim, V. N. Processing of intronic microRNAs. *EMBO J.* **26**, 775–783 (2007).
39. Morlando, M. et al. Primary microRNA transcripts are processed co-transcriptionally. *Nat. Struct. Mol. Biol.* **15**, 902–909 (2008).

40. Wu, C. L. et al. Senescence-associated long non-coding RNA (SALNR) delays oncogene-induced senescence through NF90 regulation. *J. Biol. Chem.* **290**, 30175–30192 (2015).
41. Corthesy, B. & Kao, P. N. Purification by DNA affinity chromatography of two polypeptides that contact the NF-AT DNA binding site in the interleukin 2 promoter. *J. Biol. Chem.* **269**, 20682–20690 (1994).
42. Lee, D., Nam, J. W. & Shin, C. DROSHA targets its own transcript to modulate alternative splicing. *Rna* **23**, 1035–1047 (2017).
43. Wong, N. & Wang, X. miRDB: an online resource for microRNA target prediction and functional annotations. *Nucleic Acids Res.* **43**, D146–D152 (2015).
44. Camp, R. L., Dolled-Filhart, M. & Rimm, D. L. X-tile: a new bio-informatics tool for biomarker assessment and outcome-based cut-point optimization. *Clin. Cancer Res.* **10**, 7252–7259 (2004).
45. Pawlicki, J. M. & Steitz, J. A. Subnuclear compartmentalization of transiently expressed polyadenylated pri-microRNAs: processing at transcription sites or accumulation in SC35 foci. *Cell Cycle* **8**, 345–356 (2009).
46. Schwarzenbach, H., Nishida, N., Calin, G. A. & Pantel, K. Clinical relevance of circulating cell-free microRNAs in cancer. *Nat. Rev. Clin. Oncol.* **11**, 145–156 (2014).
47. Shabman, R. S. et al. DRBP76 associates with Ebola virus VP35 and suppresses viral polymerase function. *J. Infect. Dis.* **204**(Suppl 3), S911–S918 (2011).
48. Sobhian, B. et al. HIV-1 Tat assembles a multifunctional transcription elongation complex and stably associates with the 7SK snRNP. *Mol. Cell* **38**, 439–451 (2010).
49. Li, X. D. et al. Overexpression of maelstrom promotes bladder urothelial carcinoma cell aggressiveness by epigenetically downregulating MTSS1 through DNMT3B. *Oncogene* **35**, 6281–6292 (2016).
50. Zhang, J. X. et al. Prognostic and predictive value of a microRNA signature in stage II colon cancer: a microRNA expression analysis. *Lancet Oncol.* **14**, 1295–1306 (2013).
51. Zhang, J. X. et al. Downregulation of microRNA-644a promotes esophageal squamous cell carcinoma aggressiveness and stem cell-like phenotype via dysregulation of PITX2. *Clin. Cancer Res.* **23**, 298–310 (2017).
52. Bittencourt, D. et al. Cotranscriptional splicing potentiates the mRNA production from a subset of estradiol-stimulated genes. *Mol. Cell. Biol.* **28**, 5811–5824 (2008).
53. Ran, F. A. et al. Genome engineering using the CRISPR-Cas9 system. *Nat. Protoc.* **8**, 2281–2308 (2013).
54. Montague, T. G., Cruz, J. M., Gagnon, J. A., Church, G. M. & Valen, E. CHOPCHOP: a CRISPR/Cas9 and TALEN web tool for genome editing. *Nucleic Acids Res.* **42**, W401–W407 (2014).
55. Xie, D. et al. Heterogeneous expression and association of beta-catenin, p16 and c-myc in multistage colorectal tumorigenesis and progression detected by tissue microarray. *Int. J. Cancer* **107**, 896–902 (2003).
56. Zheng, F. et al. Systemic delivery of microRNA-101 potently inhibits hepatocellular carcinoma in vivo by repressing multiple targets. *PLoS Genet.* **11**, e1004873 (2015).
57. Zheng, F. et al. The putative tumour suppressor microRNA-124 modulates hepatocellular carcinoma cell aggressiveness by repressing ROCK2 and EZH2. *Gut* **61**, 278–289 (2012).